IR Radiation from Trees to a Ski Run: A Case Study

ROSIE HOWARD AND ROLAND STULL

Department of Earth, Ocean and Atmospheric Sciences, The University of British Columbia, Vancouver, British Columbia, Canada

(Manuscript received 10 August 2012, in final form 4 February 2013)

ABSTRACT

Accurately calculating the surface radiation budget of a groomed ski run is crucial when determining snow surface temperature and other snow-related variables, knowledge of which is important for ski racing. Downwelling longwave radiation can compose a large part of the surface radiation budget in mountainous terrain. At a location on a ski run, a portion of the downwelling longwave radiation comes from the sky and a portion comes from tall evergreen trees. Infrared photographs taken during daytime at a ski run on Whistler Mountain, British Columbia, Canada, for a clear-sky day in February 2012 show that trees can enhance the downwelling longwave radiation at the center of the ski run considerably, with a maximum estimated enhancement of $75.6 \pm 16.8\,\mathrm{W\,m^{-2}}$ for trees in direct sunlight. The average needle and trunk brightness temperatures from the IR photographs were correlated with measured meteorological data. Regressions were found to allow estimation of longwave radiation from trees using nearby routine meteorological data. Absolute errors in tree longwave radiation estimations using the derived trunk and needle temperatures did not exceed $4\,\mathrm{W\,m^{-2}}$. The effect of the intervening air upon longwave radiative transfer between trees and the point of interest on the ski run was found to be small for these very short pathlengths of 50 m or less. These results can be used to improve calculations of the surface radiation budget of a groomed ski run under clear skies.

1. Introduction

Let us consider a snow-covered, groomed, and compacted ski run, known as a ski piste, on which tall evergreen trees border two sides of a slope (Fig. 1). Downwelling longwave radiation comes from a hemisphere of directions to reach a unit area in the center of the ski piste and can be measured by an upward-looking radiometer. For that same unit area, the sky downwelling longwave radiation can be reduced considerably because the full hemisphere may be blocked by trees, terrain, or other objects. Longwave irradiance from these objects may locally enhance total incoming irradiance, however (Plüss and Ohmura 1997; Sicart et al. 2006). Trees, such as the evergreens that border the ski piste, can be much warmer than the effective brightness temperature of the sky (Spittlehouse et al. 2004), especially under sunny, clear-sky conditions; thus, the trees emit a larger amount of longwave radiation per unit area. It is therefore not surprising that the longwave radiation received at the ski piste can be greatly modified by the bordering trees.

a. Downwelling longwave radiation from trees

This case study assumes that all of the reduction in sky downwelling longwave radiation is a result of the trees bordering the ski piste (see Fig. 2). For an upward-looking radiometer, the sky-view factor V_s is the fraction of hemisphere occupied by sky and the tree-view factor V_t is the remaining fraction of the hemisphere occupied by trees ($V_s + V_t = 1$).

The total downwelling longwave flux contribution from the trees received at the snow surface $L_t^{\downarrow}$ can be described by the following equation:

$$L_t^{\downarrow} = V_t(\varepsilon_t \sigma T_t^4 \mathrm{tr}_F + \varepsilon_a \sigma T_a^4), \tag{1}$$

where ε_t is the tree emissivity, $\sigma = 5.67 \times 10^{-8}\,\mathrm{W\,m^{-2}\,K^{-4}}$ is the Stefan–Boltzmann constant, T_t is the effective absolute temperature of the trees, tr_F is the flux transmittance along the path of radiation, ε_a is the flux emissivity of the intervening air between the trees and snow surface (equal to $1 - \mathrm{tr}_F$), and T_a is the absolute

Corresponding author address: Rosie Howard, Dept. of Earth, Ocean and Atmospheric Sciences, The University of British Columbia, Rm. 2020, Earth Sciences Bldg., 2207 Main Mall, Vancouver, BC V6T 1Z4, Canada.
E-mail: rhoward@eos.ubc.ca

DOI: 10.1175/JAMC-D-12-0222.1

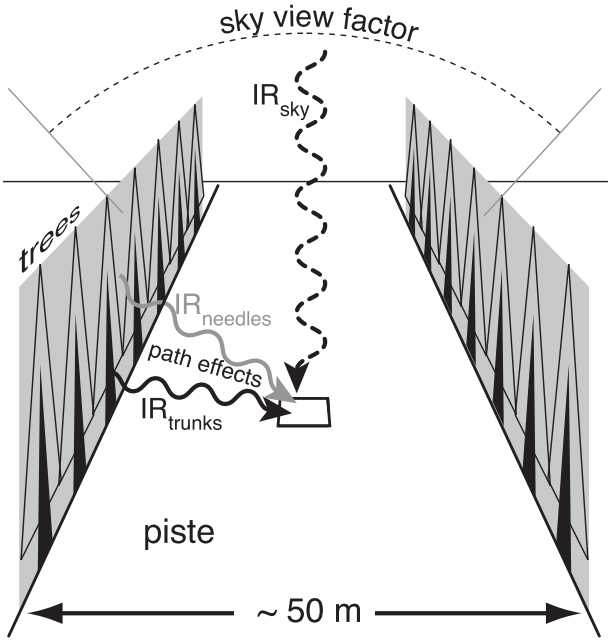

FIG. 1. Schematic showing ski piste with reduced sky view from trees, summarizing the processes examined in this case study. Here, IR_{sky}, $IR_{needles}$, and IR_{trunks} refer to infrared radiation emitted by sky, tree needles, and tree trunks, all of which contribute to the total downwelling longwave flux at the snow surface; "path effects" refers to the effect of the intervening air between the trees and the snow surface on the amount of longwave radiation received relative to that emitted.

air temperature. We define the flux transmittance as $tr_F = e^{-\tau_F}$, where $\tau_F = (5/3)k\rho\Delta s$ includes the diffusivity factor (Petty 2006), k is the mass extinction coefficient, ρ is the absolute humidity of the intervening air, and Δs is the pathlength. Note that T_a must not be confused with the effective sky temperature, which includes the cold temperatures of the upper atmosphere for clear skies. Namely, Eq. (1) incorporates the effect of the near-surface air between the trees and the snow surface on the transmission of tree longwave radiation (see "path effects" in Fig. 1).

If the effect of the air between the trees and the snow surface is neglected, then the longwave irradiance in snow-covered environments can be misestimated (Plüss and Ohmura 1997). Since water vapor is the single most important absorber in the IR band (Petty 2006), the effect depends strongly upon the humidity of the intervening air, as well as the air temperature. In general, if the air temperature between the trees and the point of interest is higher than the temperature of the trees, the radiance received at the point of interest will be greater than the blackbody radiance of the trees (Plüss and Ohmura 1997). In the appendix, we address the importance of this effect over very short pathlengths such as the width of a ski run (<50 m).

Staley and Jurica (1970) calculated values of flux emissivities for water vapor at $T_a = -10$°C and $T_a = 20$°C, from which values of k can be derived. These are also calculated and discussed in the appendix, along with estimates of the resulting change in longwave radiation.

b. Tree temperatures

Tree temperature is less commonly measured than air temperature and other meteorological variables, and therefore a relationship between the two is useful for estimating the thermal contributions from trees. Leuzinger et al. (2010) studied tree-canopy temperatures in an urban environment, for coniferous species like those found on ski pistes. They found that tree-canopy temperature was about 1°C higher than ambient air temperature. Their measurements were taken on a cloud-free day around solar noon to minimize shading, when high air–canopy temperature differences might be expected.

Leaf boundary layer resistance to heat is roughly proportional to the square root of the width of the leaf (T. A. Black 2012, personal communication). Therefore, because of their larger dimensions, broad leaves have relatively high boundary layer resistances and emit more longwave radiation than do needles under the same solar irradiance (Jarvis et al. 1976). Air–leaf temperature differences of 10°–15°C have been found for broad leaves.

Conifer needles have small boundary layer resistances (Martin et al. 1999; Jarvis et al. 1976), leading to a rapid exchange of sensible heat and a large heat transfer. This situation results in a close coupling between needle and air temperatures (Jarvis et al. 1976), and it has frequently been assumed that conifer needle temperatures rarely differ from air temperature by more than 1°C (Angell and Miller 1994; Jarvis et al. 1976; Kaufmann 1984; Tan et al. 1978). Measurements by Rutter (1967) and Vanderwaal and Holbo (1984) support this assumption, despite the difficulty in accurately measuring needle temperature (Perrier 1971).

Yamaoka (1958) found that with an incoming solar irradiance of 700 W m^{-2} (this is the approximate maximum top-of-atmosphere solar irradiance for a midlatitude site near the end of February), an air temperature of 20°C, and a relative humidity of 60%, air–needle temperature differences exceeded ±2.5°C only at wind speeds of less than 1 m s^{-1}. At a wind speed of 2 m s^{-1}, the magnitude of the air–needle temperature difference was less than 1°C. For conifers, the assumption of an air–needle temperature difference of magnitude 0°–1°C seems reasonable. This assumption is confirmed in section 3c.

Additional insight can be gained from radiation studies under quasi-uniform forest canopies. The longwave radiation can be partitioned between a sky-view

FIG. 2. For a skier going downslope, these photographs show (a) trees to the skier's right, (b) trees to the skier's left, and the view looking (c) back uphill and (d) downhill at RC Whistler. The photographs were taken in different years than that of this case study and under different conditions but are included to support the assumption that the reduction in sky-view factor at RC Whistler is mostly due to trees. [The photographs were taken by the authors at Whistler Mountain in February 2009 for (a) and April 2008 for (b)–(d).]

component (Price and Petzold 1984) and a canopy-view component, which is analogous to the tree-view component here. Despite the difference in geometry, which is generally simpler for a ski slope, the major sources of longwave radiation are identical: sky, trees, and snow.

Pomeroy et al. (2009) examined whether forest canopy warming enhances longwave radiation to snow and determined that the correct estimation of canopy temperature is essential. Likewise, it is essential to determine the effective brightness temperature of the trees on either side of a ski piste when calculating longwave radiation at the snow surface. Also, sunlit and nonsunlit trees have different radiative contributions. Sicart et al. (2004) showed that for low sun angles, cloudy environments, or shaded trees there is little opportunity for the tree temperature to differ from the air temperature, yet in sunny environments the increase in direct shortwave radiation received by trees can increase the longwave irradiance from the trees to the snow by up to 30 $\mathrm{W\,m^{-2}}$.

Tree trunks receiving direct insolation were found to be substantially warmer than the air and needle-branch temperatures. Needle temperatures were sometimes slightly warmer than air temperature. The largest differences occurred with strong insolation to discontinuous canopies, where sunlight was not extinguished until far down within the canopy or at the ground surface: the latter case is analogous to a ski piste where the sunlight entering through the clear-cut of the piste can illuminate the side of exposed trunks and branches. In general, studies that modeled tree-trunk temperatures show that incident insolation is an important consideration (Derby and Gates 1966; Potter and Andresen 2002); therefore, it is included in this case study.

Pomeroy et al. (2009) also showed that, by considering air, tree-trunk, and needle-branch temperatures separately, it is possible to reduce the mean bias in calculated incoming longwave radiation by up to fourfold relative to simply assuming that mean canopy temperature is equal to the air temperature. They use an unexplained but reasonable atmospheric emissivity of 0.6 for clear skies and 0.98 for vegetation emissivity, but the improvement between the two cases is still credible. For a groomed

ski run that has been cut through subalpine trees, it can be the case that tree trunks, branches, and needles are simultaneously visible along the ''wall'' of trees on either side of the piste, and therefore these should be considered as separate objects.

Tree emissivity varies with species (Leuzinger et al. 2010) mostly as a result of the differing components of the tree (e.g., leaves, branches, and trunk). It is frequently taken as unity (Leuzinger et al. 2010; Jarvis et al. 1976; Spronken-Smith and Oke 1998) since data are often unavailable for a particular species. For the coniferous forest canopy, Dirmhirn (1964) gives a value of $\varepsilon_t = 0.97$, and Rutter (1968) claims that this small difference from unity can lead to important differences in the emission of thermal radiation. A simple calculation shows that for tree temperatures ranging from $-10°$ to 10°C the difference in longwave radiation emitted when applying an emissivity of 0.97 versus using unity ranges from 8.2 to 10.9 $\mathrm{W\,m^{-2}}$. These values are not exceedingly large but could be significant to the energy balance.

A range of $\varepsilon_t = 0.94$–0.99 is given by Idso et al. (1969) for the emissivity of leaves among differing species, but measured values used for coniferous needles are hard to find in the literature. Jarvis et al. (1976) give values of 0.95–0.97 by drawing an analogy with the measured emissivity of broad-leaved trees and herbs (Gates and Tantraporn 1952). Since a blackbody is rarely exactly realized (Petty 2006), and for all of the above reasons, we will use $\varepsilon_t = 0.97$ for tree emissivity throughout this study.

2. Methods

For the purposes of this case study, the trees are divided into two main categories: tree trunks and tree needles (needles include branches and all material that is not trunk). The relationship between each of these and air temperature has been examined with field measurements, which are described next.

a. Site and data description

Data have been collected at a site identified as ''RC Whistler'' (50°5′16″N, 122°57′41″W) on Whistler Mountain in the southwest coastal mountain range of British Columbia, Canada; RC Whistler is in the subalpine of a recreational ski area, situated on a ski piste. For a skier facing downslope at the site, views showing trees to the skier's right and left and uphill and downhill from the site are shown in Figs. 2a–d, respectively. These photographs justify the assumption that most of the reduction in sky-view is due to trees at this site. Elevation at this point is 1335 m MSL. RC Whistler is an open active piste during winter with skiers and snowboarders during the day and Snowcat-type grooming machines at night. Skier safety precluded any permanent structures on the piste; hence, all measurements reported here use handheld/portable instruments.

A handheld FLIR Systems, Inc., E40 infrared (IR) digital camera was used to digitally record the temperature of different longwave radiation sources at RC Whistler. The camera has a field of view (FOV) of 25° × 19° and an accuracy of ±2% (up to 6°C for this case study), with a spectral range of 7.5–13 μm. A visible image is recorded at the same time as the IR image; the visible lens has an FOV of 53° × 41° to provide context for the IR image.

There are five parameters that can be input, either on the camera before the image is taken or in the analysis software afterward, to correct the temperatures that are output (160 × 120 image resolution = 19 200 temperature values per image). The FLIR software outputs the temperature of each pixel. The five input parameters are

1) the emissivity of the object being photographed,
2) the reflected apparent temperature (°C) to correct the longwave reflectivity [Radiation from surrounding terrestrial objects is reflected by the object of interest into the camera lens and can affect the measurement. This effect is mostly important when the object emissivity is low and the object temperature differs substantially from the reflected temperature. Objects considered in this study have relatively high emissivities (>0.7) and the environment in which the photographs are taken sees the same or very similar objects in all directions.],
3) the air temperature between the camera and the object (°C) as measured with a thermistor contained in a Nielsen–Kellerman Co. Kestrel 4000 Pocket Weather Tracker (hereinafter referred to as the Kestrel) with an accuracy of ±1°C,
4) the relative humidity (RH; %) of the air between the camera and the object as measured with a capacitive sensor (also part of the Kestrel) with an accuracy of ±3%, and
5) the distance between the camera and the object (m) as measured with a Nikon Corporation Forestry Pro Laser Rangefinder, which has an accuracy of ±0.46 m for ranges up to 90.5 m and ±0.91 m for ranges from 91 to 457 m.

From the center of the ski piste at RC Whistler, photographs were taken with the IR camera around a full azimuth circle, with overlapping edges to be certain that no major source of longwave radiation was omitted. The rangefinder was used to ensure repeatability of measurements (i.e., standing in the same location for each set of photographs). The first azimuth circle of photographs

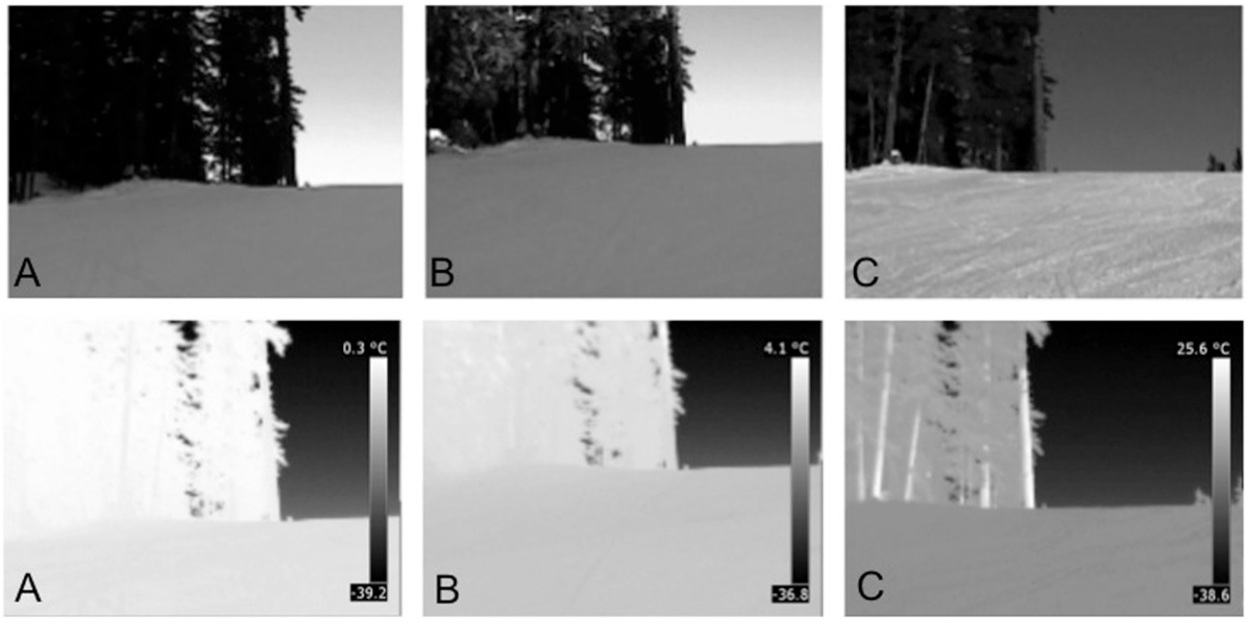

FIG. 3. (top) Visible-light photographs and (bottom) their paired (case pairs are referred to by their corresponding letter labels) IR photographs taken at RC Whistler, including trees, sky, and ski piste, under clear skies, as described in Table 1. All photographs are looking in approximately the same direction for comparison. Note that the temperature scale on each IR picture is different since it is set by the FLIR software for each picture individually. On the scale in the IR photographs, white is warmer and black is colder. (The photographs were taken by the authors at Whistler Mountain for the case-study day of 3 Feb 2012.)

was taken with an approximate elevation angle of 0°, relative to the slope of the ski piste. The process was repeated for increasing elevation angles until all terrestrial sources of longwave radiation were captured, most of which were trees.

The sky was photographed for comparison, mostly in pictures that also included trees. The sky condition across all photographs is clear skies. For this case study at RC Whistler, three sets of photographs were taken on 3 February 2012. One full set of photographs captures all of the trees (and terrain) in the upper-hemispheric view above a plane level with the piste, some of the sky, and some of the ski slope itself. These photographs show the brightness temperatures of different tree components and of the sky under various conditions as described in section 2b. The rangefinder was also used to find the average width of the ski run at RC Whistler, which is 45.8 m.

The following data were also observed manually at the beginning and end of each set of photographs: air temperature and RH from the Kestrel; wind speed from the propeller anemometer contained in the Kestrel, with accuracy of ±3%; approximate wind direction (i.e., up/down/across the slope from the ribbon telltale attached to the Kestrel); cloud cover, cloud type, and approximate cloud height(s); precipitation/fog (measurements with the IR camera will be affected because radiation will be received from precipitation and fog particles rather than from trees and other terrestrial objects of interest); sun on snow/trees (also observed in digital camera images); and piste snow surface conditions (groomed/hard packed/soft packed/fresh powder/dry/moist/melting).

These data will be used to investigate the relationship between air temperature and the temperature of different tree components (trunks and needles). A Taylor Precision Products Co. 806E4L digital temperature probe (accuracy of ±1°C) was hung in the shade on a nearby tree at least 1 m from the trunk and was read manually just before and after every photograph set. This gave six data points from the probe that were used to validate the Kestrel air temperature measurements.

b. Data analysis

Infrared camera pictures were studied by eye to identify whether different tree components did in fact have different effective brightness temperatures and to compare them with other sources of radiation such as the sky. Figure 3 shows pairs of visible and IR photographs taken looking uphill and toward the trees on a skier's right at RC Whistler. Photographs were taken on 3 February 2012, when the average air temperature was 3.6°C with clear skies and a light, consistent downslope wind. No precipitation fell on this day.

TABLE 1. Cases illustrated by photographs in Fig. 3, for the RC Whistler site at 50°5′16″N, 122°57′41″W.

Photograph reference	Time taken (PST)	Date (2012)	Trees in sun or shade	Snow on trees	Sky condition
A	1012	3 Feb	Shade	No	Clear
B	1059	3 Feb	Sun and shade	No	Clear
C	1308	3 Feb	Sun	No	Clear

Each photograph is described in Table 1. For the IR photographs, pixel temperature was extracted using FLIR software. The ''distance between camera and object'' parameter in the software was set to zero to remove the built-in distance-correction algorithm for absorption/emission by air along the path, and the object emissivity was set to 1. Both of these parameters are corrected in the postanalysis.

A histogram of the temperatures from all pixels in each IR photograph was used to identify frequency maxima, the temperatures of which were matched with objects in the photograph (tree trunks, needles, ski piste, etc.). This procedure allowed the average temperature of these objects to be calculated and allowed different emissivities to be applied to different objects (trees and sky). Figure 4 (bottom) shows the histogram for IR photograph A from Fig. 3. Also plotted in Fig. 4 is the array of pixel temperatures (top-left panel) and the same data contoured by thresholds, to verify that these peaks are placed well (top-right panel).

A sensitivity test was conducted to assess how the average temperatures of objects varied with a changing averaging threshold. When varying the thresholds by 1°C, the changes in average object temperature are at least one order of magnitude smaller than the observed differences between object temperatures. Note that the measurement of sky temperature is limited by the FLIR camera, which cannot be calibrated below −40°C. Measurements below −40°C are truncated to this value. Where measured sky temperatures are used in the data analysis, the temperatures were greater than −40°C, and therefore results are not affected by any truncation.

Needle and trunk temperatures were measured and extracted as described above for each photograph in every direction. Raw output from the IR camera was adjusted to remove the effects of the intervening air using measurements of air temperature and humidity (see section 1a). The maximum adjustment to needle temperature was 0.1°C. The maximum adjustment to trunk temperature was 3.0°C. Direct insolation onto an idealized cylindrical tree trunk at the center of the ski

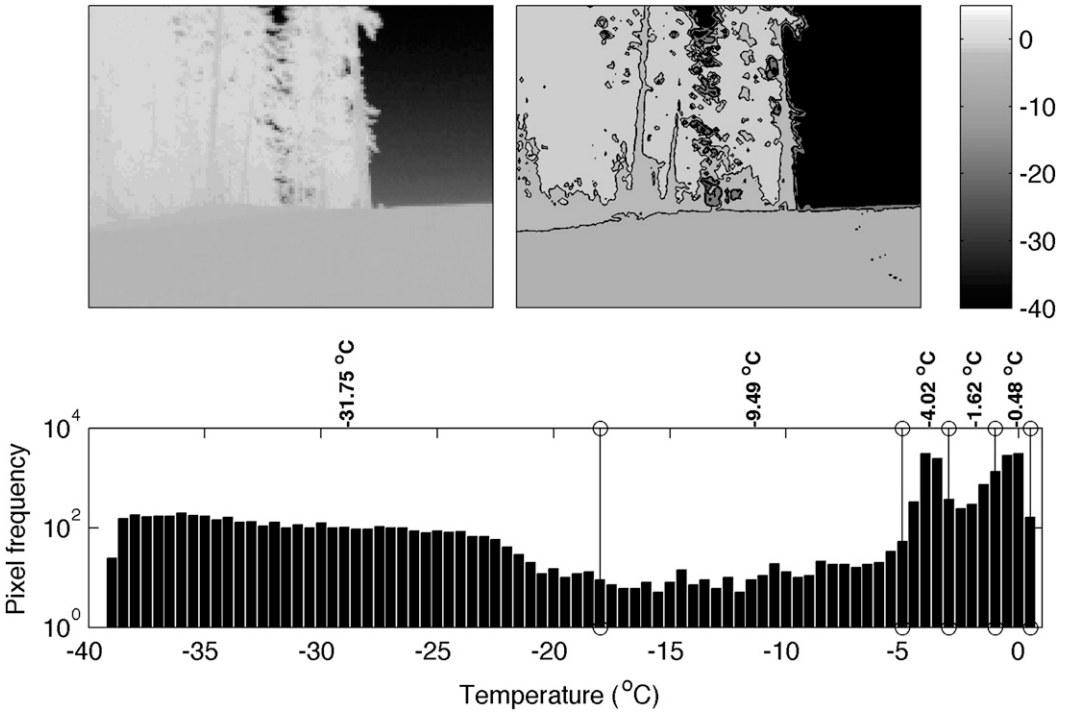

FIG. 4. (top left) Plotted temperature array of IR photograph A from Fig. 3, (top right) the same data contoured by the chosen thresholds to indicate that they isolate the features claimed (trunks, needles, piste, and sky), and (bottom) histogram of the same data that were used to identify the frequency maxima.

piste was also calculated by using equations from Howard and Stull (2011) and Potter and Andresen (2002).

One goal of this analysis is to quantify the thermal contributions from trees for RC Whistler under clear skies. We do this for direct sunlight in the middle of the day to estimate a hypothetical maximum enhancement for this case study. For a flat surface, the incoming longwave radiative flux from the sky $L_s^{\downarrow}$ can be written as

$$L_s^{\downarrow} = \varepsilon_s \sigma T_s^4, \tag{2}$$

where ε_s is an effective sky emissivity, $\sigma = 5.67 \times 10^{-8}\,\mathrm{W\,m^{-2}\,K^{-4}}$ is the Stefan–Boltzmann constant, and T_s is an effective absolute temperature of the sky. Sky emissivity has been shown to vary from approximately 0.7 for a clear sky in alpine environments (Kuhn 1987) to approximately unity for an overcast sky.

There are a number of parameterizations available that use screen-height measurements of air temperature and vapor pressure to calculate clear-sky emissivity and an effective sky emissivity that is based on fractional cloud cover. Sedlar and Hock (2009) present a comprehensive review of the parameterizations. In general, clear-sky emissivity scattered around 0.7, consistent with several other studies (Konzelmann et al. 1994; Kuhn 1987; Marty and Philipona 2000), and therefore sky emissivity was set to 0.7 for this case study.

By considering the weighted thermal contributions from sky [Eq. (2)] and trees [Eq. (1)], the total downwelling longwave radiation at the surface of the ski run $L^{\downarrow}$ can be expressed as

$$L^{\downarrow} = V_s \varepsilon_s \sigma T_s^4 + V_t \varepsilon_t \sigma T_t^4, \tag{3}$$

and further as

$$L^{\downarrow} = V_s \varepsilon_s \sigma T_s^4 + V_t \varepsilon_t \sigma [f_T T_{\mathrm{tr}}^4 + (1 - f_T) T_n^4], \tag{4}$$

where f_T is the trunk fraction, defined as the fraction of the "walls" of trees that is trunk; T_{tr} is the absolute trunk temperature; and T_n is the absolute needle temperature. Accurate estimation of the sky-view factor is crucial for accurate estimates of $L^{\downarrow}$ (Sicart et al. (2006). According to Plüss and Ohmura (1997), the error from calculating the incoming longwave radiation as in Eq. (3) is similar to the error assumed for radiation instruments, assuming isotropic radiance from the sky and terrain. The sky-view factor for this case study is calculated from Müller and Scherer (2005):

$$V_s = \frac{1}{N} \sum_{i=1}^{N} (1 - \sin\theta_{h,\phi_i}), \tag{5}$$

where θ_{h,ϕ_i} is the horizon-elevation angle computed or measured for N discrete azimuth angles ϕ_i, $i = 1, N$. Larger N gives a more accurate sky-view factor. Using a theodolite survey (Howard and Stull 2011) with $N = 72$ (every 5° azimuth), the sky-view factor at RC Whistler has been calculated as $V_s = 0.65$. The error associated with this calculation is considered in section 3b.

To estimate the potential downwelling longwave enhancement due to trees for this case study at RC Whistler, the IR photograph with the greatest temperature difference between trees (needles and trunks) and sky was selected by using the histogram analysis described above. Using these measured trunk, needle, and sky temperatures, the total downwelling longwave radiation was calculated using Eq. (4). This is intended to quantify the potential longwave enhancement due to trees on a sunny day in February at RC Whistler.

Given that the needles and trunks can be clearly segregated by their temperatures in the histogram analysis for photograph C (not shown), the trunk fraction can be calculated as 0.12. The photographs for case C show just a small part of all of the trees at RC Whistler, and so it is possible that f_T is larger than this. Needles make up the largest proportion of the walls of evergreen trees at RC Whistler, as seen in Figs. 2 and 3, and it is unlikely that f_T is greater than 0.5, and therefore this value was chosen as an upper bound.

The total downwelling longwave radiation was calculated as described above for sky view ranging from 0 to 1 and for f_T ranging from 0 to 0.5, in increments of 0.1. The trunk and needle emissivity was set to 0.97. The thermal calculations including trees are compared with the case with sky only for the same effective sky temperature but with no trees (i.e., $V_s = 1$) to establish the relative importance of including the trees. Results are reported in section 3a.

A second goal of this analysis is to find parameterizations for needle and trunk temperatures, assuming they should be treated separately, that use routine meteorological data. This goal is practically important since meteorological measurements are generally more widely available than measurements of tree temperature. The corrected object temperatures from all photographs taken on 3 February 2012 were analyzed with concurrent meteorological data, and the results are discussed in section 3c.

3. Results

a. Observations

All IR photographs in Fig. 3 show that the sky is much colder than the tree trunks and needles. Infrared photograph C has diffuse and direct sunlight shining on the trees, and tree trunks are clearly identified as the warmest

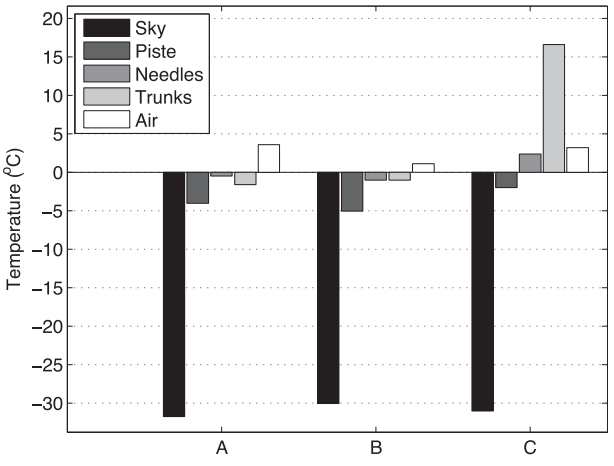

FIG. 5. The average temperature of each ''object'' for cases A–C shown in Table 1.

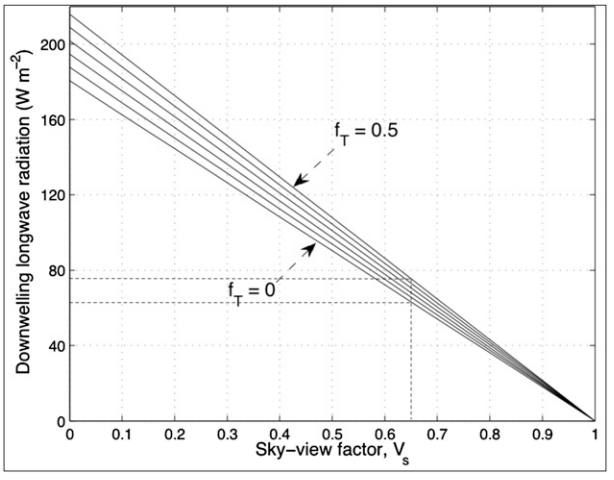

FIG. 6. Plot showing difference between downwelling longwave radiation including trees (amount of trees signified by sky-view factor V_s) and downwelling radiation for sky alone, for IR photograph C. The different lines show how the difference varies for different trunk fractions f_T from 0 to 0.5, in 0.1 increments. Factor $V_s = 0.65$ at RC Whistler.

objects. Photographs A and B have the trees in the shade and show a much more uniform tree temperature across needles and trunks.

Figure 5, which is based upon the histogram analysis that is described in section 2b, displays the average brightness temperature of different objects in photograph pairs A–C. In all cases, needles and trunks are warmer than the sky, supporting the findings of Spittlehouse et al. (2004). The maximum brightness temperature difference between needles and sky is 33.4°C, and that between trunks and sky is 47.6°C (photograph C) when the sky is clear and there is direct sunlight on the trees. This result translates into differences in emitted longwave radiation of 180.5 and 251.3 W m^{-2}, respectively, calculated with $\varepsilon_s = 0.7$ and $\varepsilon_t = 0.97$.

In the case of direct sunlight and clear sky, the trunk average brightness temperature reaches nearly 17°C (Fig. 5). This indicates a potentially significant source of radiation but is reduced by considering f_T.

Photograph C shows the greatest brightness temperature difference between trees (needles and trunks) and sky. The trees are in direct sunlight at this time [1308 Pacific standard time (PST)], which is only 42 min after the maximum solar radiation input on 3 February 2012 [using equations from Howard and Stull (2011)]. This is the justification for using measurements from this photograph to estimate an approximate maximum bound on the longwave radiative contribution from trees for this case study.

The difference between the total downwelling longwave radiation from sky alone and the total downwelling longwave including trees and varying V_s from 0 to 1, as described in section 2b, is given in Fig. 6. Assuming that all of the reduction in sky view is due to trees on either side of the ski run and using the measured sky-view factor of 0.65 for RC Whistler, it is shown in Fig. 6 that a considerable increase in downwelling longwave radiation from 63.2 W m^{-2} ($f_T = 0$) to 75.6 W m^{-2} ($f_T = 0.5$) is possible for this case study. Several errors associated with this simplified model [Eq. (4)] need consideration and are discussed next.

b. Error analysis

Equations (3) and (4) incorporate errors that are due to 1) estimation of the sky- and tree-view factor, 2) estimation of the sky and tree emissivity, and 3) measurements of tree (trunk and needle) and sky temperature. The following list expands upon these three sources of error.

1) Errors in theodolite measurements used to calculate the sky-view factor at RC Whistler are difficult to quantify. RC Whistler was surveyed at every 5° of azimuth, resulting in discontinuities. We also made the assumption that all of the reduction in sky view is due to trees, when in reality there was a small number of other objects (e.g., snow-covered rocks) contributing to the total downwelling longwave radiation. In an attempt to quantify this situation, in addition to showing results for the sky-view factor ranging from 0 to 1 in Fig. 6, we assumed an uncertainty of ±2° for theodolite readings in each of the 72 azimuth directions (see Howard and Stull 2011). Horizon-elevation-angle readings were reported to 0.5° precision, and therefore we feel this estimate is reasonable.

The resulting uncertainty in the sky- and tree-view factor is ±0.03 (dimensionless).

2) Again, errors in sky and tree emissivity are difficult to quantify since we chose values from the literature. To incorporate the anisotropy of the sky and tree radiation, and using ranges from the literature discussed here as guidance, we use $\varepsilon_s = 0.7 \pm 0.05$ and $\varepsilon_t = 0.97 \pm 0.03$ (dimensionless).
3) The FLIR camera used to measure sky and tree temperature reports an uncertainty of ±2% (~±5 K for the absolute temperatures measured here).

We acknowledge that the first and second sources of errors discussed above include assumptions, but nonetheless we include them for an estimate of the overall error propagation. The resulting increase in downwelling longwave radiation due to incorporating thermal emissions from the surrounding trees is reported as a possible range from $63.2 \pm 14.8\,\mathrm{W\,m^{-2}}$ ($f_T = 0$) to $75.6 \pm 16.8\,\mathrm{W\,m^{-2}}$ ($f_T = 0.5$) for this case study. Even with this uncertainty, the overall increase in total downwelling longwave radiation is substantial.

c. *Parameterizations for needle and trunk temperature*

Infrared photograph C in Fig. 3 shows a large difference between trunk and needle brightness temperature of 14.2°C with direct sunlight and a sun elevation angle of 22.5°. There is no scattering because of clouds and no snow on the branches. This picture was taken about 40 min after solar noon with the sun directly behind the photographer so that solar radiation is near maximum for the day. The maximum temperature differences seen here support the findings of Martin et al. (1999) and Jarvis et al. (1976) that needles have low boundary layer resistances for heat transfer while trunks do not.

Infrared photographs A and B corroborate this assertion. The needles and trunks in photograph B cannot easily be distinguished from each other where they are in the shade. The sun is rising just above the local horizon at this time and there are some needles in the sun that are slightly warmer than the rest. There is no snow on the needles and the sky is clear. Photograph A is taken 47 min earlier and the trunks are actually colder than the needles. It is possible that warming has begun from diffuse sunlight and heat is being more rapidly transferred to the needles than the trunks.

In addition, the average brightness temperature of the needles varies by only 3.4°C across all three cases as compared with a variation of 18.2°C in the average trunk brightness temperature. This small range in needle temperature again implies rapid heat transfer to/from the air for needles but not for trunks.

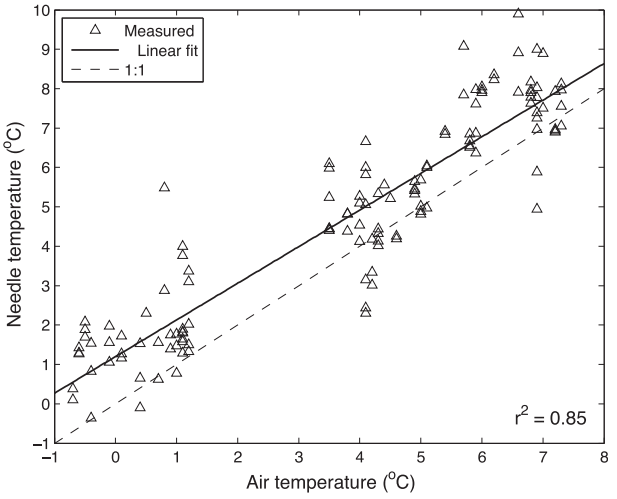

FIG. 7. Air temperature vs needle temperature for 3 Feb 2012, with the linear regression line (solid) and the 1:1 line (dashed) shown.

1) NEEDLE TEMPERATURE

For 3 February, there is a linear correlation between air and needle temperature (Fig. 7; correlation coefficient squared $r^2 = 0.85$), with best fit given by

$$T_n = 1.20 + 0.93T_a, \tag{6}$$

where T_n is needle temperature. This is found by using measured needle temperatures from all photographs and the concurrent air temperatures. Equation (6) is in good agreement with Leuzinger et al. (2010). By adding RH and wind speed U measurements in a multiple linear regression, r^2 improves slightly to 0.88:

$$T_n = 17.92 + 0.22T_a - 0.18\mathrm{RH} + 0.16U, \tag{7}$$

where T_a is in degrees Celsius, RH is in percent, and U is in meters per second.

The mean wind speed on 3 February 2012 is $2.2\,\mathrm{m\,s^{-1}}$. Despite some solar radiation incident on the Kestrel on this day, it seems that it was ventilated sufficiently by the ambient wind to provide reasonable temperature measurements, giving the linear relationship that was observed and a somewhat normal distribution of air–needle temperature difference (Fig. 8). The mean difference between the Kestrel and Taylor temperature measurements on 3 February is 0.2°C, also implying reliable air temperature measurements.

With use of the Stefan–Boltzmann law with $\varepsilon_t = 0.97$, the mean absolute error (MAE) and root-mean-square error (RMSE) in emitted longwave radiation are 3.65 and $4.60\,\mathrm{W\,m^{-2}}$, respectively, as a result of the temperature errors when using Eq. (6). By including the tree-view

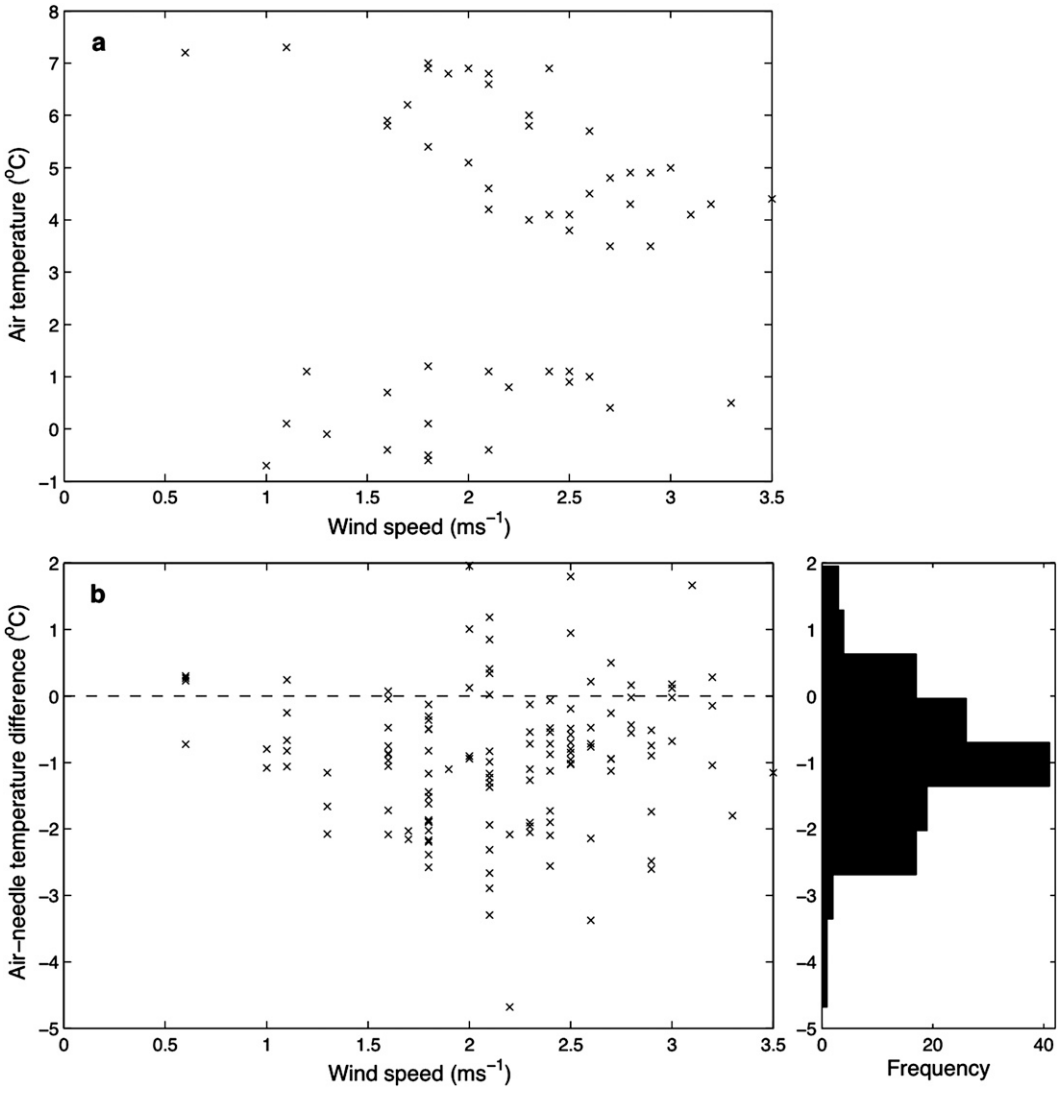

FIG. 8. (a) Wind speed vs air temperature and (b) wind speed vs air–needle temperature difference for 3 Feb 2012.

factor (0.35) and assuming all needles (no trunks) to estimate maximum error, these are each reduced to 1.28 and 1.61 W m^{-2}.

2) TRUNK TEMPERATURE

Trunk temperature was much more variable than needle temperature in general (standard deviations of 7.51° and 2.64°C, respectively). For this reason, the data were smoothed using a moving average with a window size of approximately 5 min. The window size is slightly variable in time since the photographs were taken manually and not at completely regular intervals. The estimated trunk temperature is described by

$$T_{\mathrm{tr}} = 8.29 + 1.86T_a - 0.02\mathrm{RH} + 1.55U, \qquad (8)$$

where T_{tr} is trunk temperature and the other variables and units are as before. Figure 9 shows a reasonable linear correlation ($r^2 = 0.86$) between the estimated trunk temperature and the smoothed trunk temperature data for 3 February. The errors in emitted longwave radiation as a result of the temperature errors (between estimated and raw measured trunk temperature) were calculated, with MAE = 19.78 W m^{-2} and RMSE = 26.64 W m^{-2}. These values initially appear significant; when once again the tree-view factor (0.35) and the maximum trunk factor (0.5) are taken into consideration, however, these errors are reduced to 3.46 and 4.66 W m^{-2}, respectively. Adding incident solar radiation to the regression made the trunk temperature estimate much worse, with $r^2 = 0.12$. Figure 10 suggests that

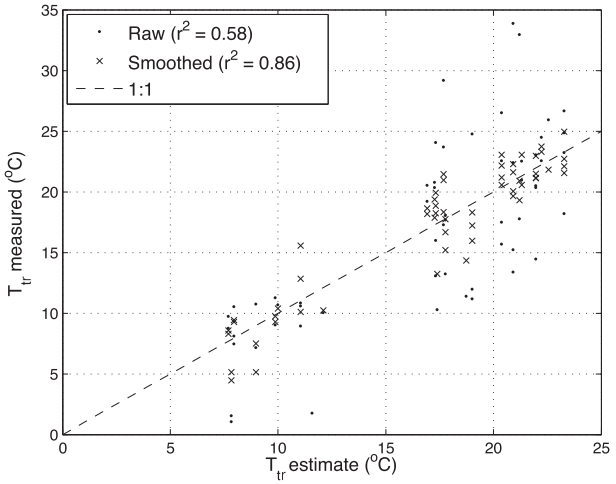

FIG. 9. Estimate of tree-trunk temperature vs measured trunk temperature for data from 3 Feb 2012, with 1:1 line (dashed) shown. Black dots indicate raw trunk temperature data, and times signs indicate smoothed trunk temperature data.

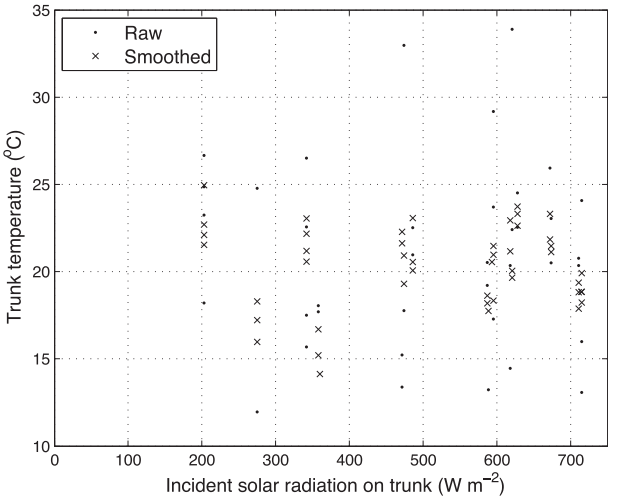

FIG. 10. Solar radiation incident on tree trunk vs trunk brightness temperature. Black dots indicate raw trunk temperature data, and times signs indicate smoothed trunk temperature data.

the solar influence has been captured by the other variables already in the regression.

There are other factors that contribute to the imperfect correlations seen here. The definition of ''needles'' here assumes that everything that is not trunk is needle. In reality, this is not the case: there are smaller branches and twigs as well as other plants. These other ''objects'' may not have small boundary layer resistances like needles do and may, therefore, not transfer heat as efficiently.

4. Relationship to urban canyons

An analogy for a ski slope with tall trees on either side is that of an urban canyon, with the buildings representing the trees and the canyon floor representing the ski piste. Nunez and Oke (1977) note that the most active surfaces of an urban canyon change with time. The downwelling longwave enhancement by trees estimated from measurements at RC Whistler is for a special case for trees in direct sunlight. The azimuth orientation of the RC Whistler piste centerline is 225°, which means that for 3 February the sun shone on all trees at about 1505 PST.

A numerical study by Arnfield (1990) showed that under clear skies the largest canyon wall irradiances were found for the smallest aspect (height to width) ratios in winter when the sun is low. This result is not surprising since the sun has a much lower elevation angle in winter and, therefore, a high angle of incidence to a vertical surface, so long as it is not shadowed in a canyon with a large aspect ratio.

For RC Whistler, later in the day when the sun reaches 225° azimuth (and all trees are in direct sunlight), the solar angle of incidence to the trees is higher, implying that the longwave enhancement from trees could be larger than was estimated for this case study. This possibility emphasizes that the orientation of a ski piste is important in determining longwave enhancement as a result of incoming shortwave radiation under clear skies.

For this case study on 3 February 2012, the top-of-atmosphere incoming shortwave radiation is calculated as 540 W m^{-2} [using equations from Howard and Stull (2011)] at the time that IR photograph C was taken (1308 PST). Just 1 month later (1 March), the maximum top-of-atmosphere incoming shortwave radiation would increase to approximately 740 W m^{-2}, potentially resulting in warmer trunk, needle, and air temperatures and, hence, greater longwave enhancement.

In addition, later in the winter when we expect larger incident solar radiation for clear skies, the sun reaches 225° azimuth at an earlier time of day, meaning the solar heating effect could be even stronger. This effect is likely counteracted by the solar elevation also being larger earlier in the day and therefore reducing the angle of incidence to the vertical trees, however. In general, urban canyon studies suggest that the decreased sky-view factor (for a center point on the urban canyon floor) reduces the power of the sky as a radiative sink (Nunez and Oke 1976) and, therefore, also as a source.

5. Conclusions

a. Summary

When calculating the total downwelling radiation for a groomed ski piste, the enhancement of downwelling

longwave radiation from trees is significant in clear-sky conditions, as expected. This case study suggests that it is crucial to include the longwave radiation emitted by trees for clear skies and when the trees are in direct sunlight. For the beginning of February at RC Whistler, a maximum longwave radiation enhancement due to trees of $75.6 \pm 16.8\,\mathrm{W\,m^{-2}}$ was estimated for clear-sky conditions with no snow on the trees. Later in winter, the longwave enhancement could be larger in clear-sky conditions because of greater incoming shortwave radiation resulting in higher tree temperatures.

When in direct sunlight, tree trunks can be significantly warmer than needles and sky, thereby becoming a potentially large source of longwave radiation. The trunk fraction becomes important in this situation, and the trunks must be treated separately from the needles when determining longwave enhancement. The error in neglecting the trunks is less than the error in neglecting the trees altogether, however, because the trunk fraction is small.

Air temperature measurements were found to be sufficient to approximate needle temperature under clear skies, since needles have low boundary layer resistances. Estimates can be slightly improved by adding measurements of relative humidity and wind speed in a multiple linear regression.

A linear relationship between trunk temperature and air temperature, relative humidity, and wind speed was also found for clear skies. Adding in incident solar radiation for the clear-sky case did not help, possibly because the solar effect was represented by the other meteorological variables already in the regression. The errors in emitted longwave radiation as a result of the temperature errors between the trunk temperature estimate and raw measured data initially look large, but the sky-view factor and trunk factor reduce them significantly (tree-view factor $\times$ maximum trunk fraction $= 0.35 \times 0.5 = 0.175$), making the relationship robust and suitable for the purposes of this study.

b. Recommendations

On the basis of this case study, it is recommended that, when approximating the downwelling longwave radiation for a ski piste, the sky view must be calculated and the longwave radiation from the trees must be included. This is important for clear skies, sun on trees, and no snow on trees.

For clear skies, equations similar to Eqs. (7) and (8) can be used to calculate needle and trunk temperature, respectively. If relative humidity and wind speed data are not available, an equation similar to Eq. (6) can be used for needle temperature with a small decrease in accuracy. It is not recommended to use these relationships in cloudy conditions.

In considering the effects of the air between the trees and the ski piste (see the appendix), the choice of mass extinction coefficient k is more crucial for warmer air temperatures and higher humidities. For cold weather, a value of $k = 0.3\,\mathrm{m^2\,kg^{-1}}$ is reasonable over the pathlength $\Delta s = 20\,\mathrm{m}$ for this case-study site. The effect of the air was found to be small over this pathlength. The surface radiation and energy balance over snow are notoriously difficult to calculate, however, and therefore when relevant data are available to make these small corrections to the incident longwave flux it is desirable to include them.

c. Future work

More data, like those collected in this study, should be gathered on overcast and cloudy days to determine a relationship between tree (trunk and needle) temperature and air temperature under these conditions. There appears to be a gap in the literature regarding the value of the water vapor mass extinction coefficient for pathlengths from zero to tens of meters. This is perhaps because there is less desire to calculate radiative transfer over these short distances or because the effects of the air are small for these pathlengths. Future work could include flux emissivity measurements or modeling using a rapid radiative transfer model to calculate the behavior of k for distances from zero to tens of meters. Most important, this work can be used to improve calculations of the piste surface radiation budget and, in turn, the surface heat budget. Such work is critically important for calculating piste conditions relevant to ski racing, such as the temperature of the snow surface and the snow liquid water content. These variables are used by ski technicians to make decisions about which skis to use and how to wax them. It may be possible and is definitely desirable, with input of atmospheric variables, to produce forecasts of snow-surface temperature from the surface heat budget so that ski technicians have this knowledge ahead of race time.

Acknowledgments. Funding was provided by Own the Podium 2010, with special thanks given to Dr. Todd Allinger, the Vancouver Olympic Committee, the Natural Sciences and Engineering Research Council of Canada, and the Geophysical Disaster Computational Fluid Dynamics Center of The University of British Columbia. We thank Emilie Benoit for carefully completing so many histogram analyses. Also, we thank Dr. Thomas Nipen, George Hicks, and Bruce Thomson of the Weather Forecast Research Team of The University of British Columbia for their valuable input.

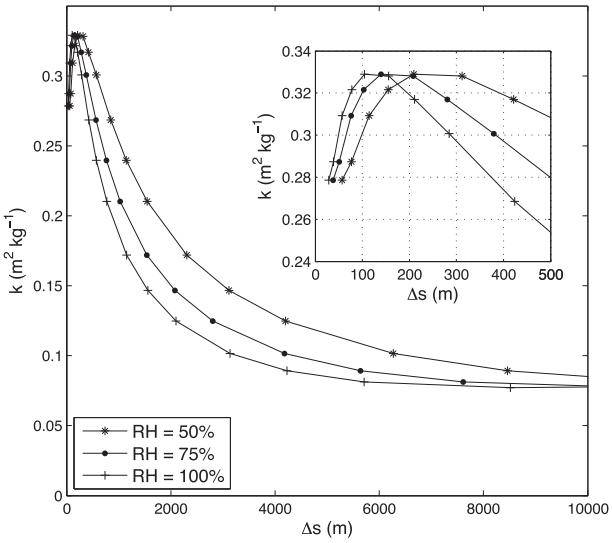

FIG. A1. Mass extinction coefficient k vs pathlength Δs for $T_a = -10°C$ and RH = 50%, 75%, and 100%. The zoomed inset shows how k varies for short pathlengths, Δs = 0–500 m, and that the literature values are not defined down to Δs = 0 m. The data are derived from SJ1970.

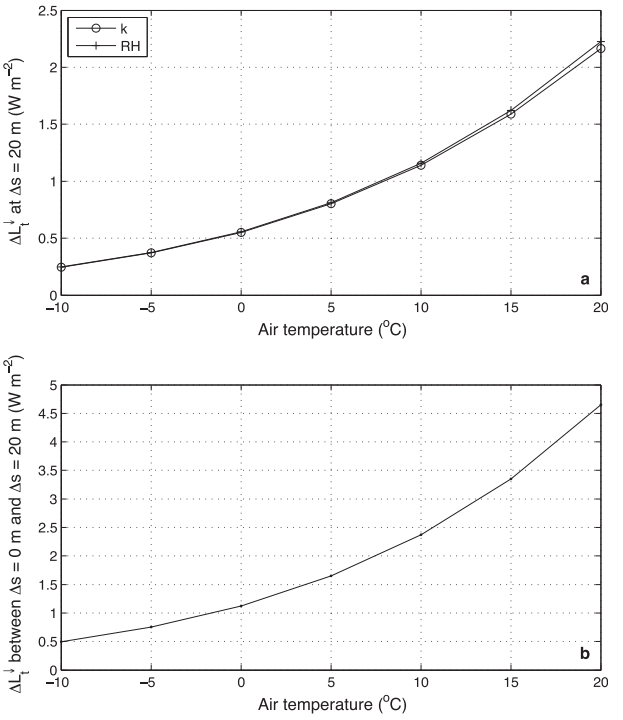

FIG. A2. (a) The difference in longwave radiation transmitted by trees over the ranges $0.20 \le k \le 0.35\,m^2\,kg^{-1}$ and 50% ≤ RH ≤ 100% for varying air temperatures for $\Delta s = 20$ m, calculated using Eq. (1) with $V_t = 1$. (b) The difference between downwelling longwave radiation from trees including the effects of the air over $\Delta s = 20$ m and neglecting them ($\Delta s = 0$ m). When the air is included, it is saturated (RH = 100%) and $k = 0.3\,m^2\,kg^{-1}$.

APPENDIX

Effect of Humidity and Mass Extinction by Air on Longwave Radiation from Trees to Piste

This appendix investigates whether air along the path between the trees and the snow surface can significantly modify the IR radiation reaching the piste from the trees.

a. Calculations from the literature

Flux emissivities from Staley and Jurica (1970, hereinafter SJ1970) are used along with typical values of air temperature and relative humidity for RC Whistler to study the effect of the intervening air on the longwave radiation transmitted by the trees to the piste surface. The inset in Fig. A1 shows values of mass extinction k for water vapor derived from SJ1970 for $T_a = -10°C$; RH = 50%, 75%, and 100%; and Δs = 500 m. SJ1970 show how flux emissivities vary with ''water-vapor path length'' u, where $u = \rho_v \Delta s$; ρ_v is absolute humidity, and therefore Δs appears to vary with ρ_v. Distances on the order of the width of the ski piste at RC Whistler (~50 m) are important to this study.

These pathlengths are not covered by the SJ1970 derived values of k, which have a lower limit in Δs (see Fig. A1, inset). From the SJ1970 data for Δs = 0–500 m, RH = 50%–100%, and $T_a = -10°C$, the mean k value is $0.3\,m^2\,kg^{-1}$. To validate this choice, the longwave flux was calculated using Eq. (1) with $k = 0.3\,m^2\,kg^{-1}$, for $T_a = -10°C$ and RH = 50%–100%, and for Δs = 0–60 m (the ''gap'' in the SJ1970 values). This calculation gave longwave radiation values that extend from the appropriate surface value (in the limit of Δs = 0 m) and match up well with longwave radiation values derived from SJ1970 (not shown) for the longer pathlengths, as seen in Fig. A1. It is possible that k continues to vary below the lower limits of Δs in SJ1970, but investigation of such behavior is outside the scope of this study.

b. Sensitivity tests

Two sensitivity tests were conducted to help to determine the effect of air humidity and choice of k over the path of longwave radiation. First, longwave radiation was calculated with $k = 0.3\,m^2\,kg^{-1}$ for RH = 50%, 75%, and 100%, and for T_a varying from − 10° to 20°C in 5°C increments. Second, a range of values of k was chosen on the basis of the data in Fig. A1 for short pathlengths: k = 0.20, 0.25, 0.30, and $0.35\,m^2\,kg^{-1}$. For the same air temperatures as in the first test, the longwave flux was calculated with these k values for RH = 100%. Figure A2 shows the maximum difference in longwave radiation for each air temperature as a result

of varying k and RH over the stated ranges, for Δs = 20 m, which is roughly the distance from the trees to the center of the ski piste at RC Whistler.

To establish the error in longwave radiation from the trees in the case in which appropriate measurements were not available to include the effects of the air, the flux was calculated with and without these corrections, for $k = 0.3\,\mathrm{m^2\,kg^{-1}}$ and RH = 100%. An RH of 100% was chosen since this gives the maximum attenuation in longwave radiation due to water vapor for each temperature (i.e., maximum possible ρ_v at each temperature). Longwave radiation emitted from trees is calculated for air temperatures from $T_a = -10$°C to $T_a = 20$°C (in 5°C increments) and for effective tree temperatures of $T_t = T_a + 5$°C with an effective tree emissivity of $\varepsilon_t = 0.97$. The rate at which the radiation attenuates per meter is proportional to $k\rho_v$ and does not depend upon the temperature difference between the air and the trees.

c. Results

The sensitivity tests for k and RH showed that the difference in longwave radiation due to varying these over the ranges chosen approximately doubles for every 10°C increase in T_a (Fig. A2a). In winter, when ski racing occurs, air temperature is usually below freezing. Therefore, a maximum error of $0.55\,\mathrm{W\,m^{-2}}$ would result from varying k for pathlengths up to Δs = 20 m. The same error is seen from varying RH between 50% and 100%. This result suggests that the choice of k is more important for warmer (summer) air temperatures and that it is more crucial to include the effects of the air for higher humidities. For the cold temperatures in this study, however, the precise value of k within the range given is less important.

Figure A2b shows the difference in longwave radiation from the trees between including the effects of the air (for Δs = 20 m) and neglecting them (Δs = 0 m). Again the error increases for higher temperatures. The error in including the effects of air and using an incorrect k value, within the bounds tested here, is always less than that if the air effects are completely neglected. Also, the errors in completely neglecting air effects are one or two orders of magnitude smaller than the errors in neglecting the longwave contribution from the trees under clear skies.

REFERENCES

Angell, R. F., and R. F. Miller, 1994: Simulation of leaf conductance and transpiration in *Juniperus occidentalis*. *For. Sci.,* **40,** 5–17.

Arnfield, A. J., 1990: Street design and urban canyon solar access. *Energy Build.,* **14,** 117–131.

Derby, R. W., and D. M. Gates, 1966: The temperature of tree trunks—Calculated and observed. *Amer. J. Bot.,* **53,** 580–587.

Dirmhirn, I., 1964: *Das Strahlungsfeld im Lebensraum* (*The Radiation Field in the Environment*). Akademische Verlagsgesellschaft, 426 pp.

Gates, D. M., and W. Tantraporn, 1952: The reflectivity of deciduous trees and herbaceous plants in the infrared to 25 microns. *Science,* **115,** 613–616.

Howard, R., and R. Stull, 2011: Forecasting sun versus shade in complex terrain for the 2010 Winter Olympic and Paralympic Games. *Bull. Amer. Meteor. Soc.,* **92,** 1303–1309.

Idso, S. B., R. D. Jackson, W. L. Ehrler, and S. T. Mitchell, 1969: A method for determination of infrared emittance of leaves. *Ecology,* **50,** 899–902.

Jarvis, P. G., G. B. James, and J. J. Landsberg, 1976: Coniferous forest. *Vegetation and the Atmosphere: Vol. 2. Case Studies,* J. L. Monteith, Ed., Academic Press, 171–240.

Kaufmann, M. R., 1984: A canopy model (RM-CWU) for determining transpiration of subalpine forests. I. Model development. *Can. J. For. Res.,* **14,** 218–226.

Konzelmann, T., R. S. W. van de Wal, W. Greuell, R. Bintanja, E. A. C. Henneken, and A. Abe-Ouchi, 1994: Parameterization of global and longwave incoming radiation for the Greenland ice sheet. *Global Planet. Change,* **9,** 143–164.

Kuhn, M., 1987: Micro-meteorological conditions for snowmelt. *J. Glaciol.,* **33,** 24–26.

Leuzinger, S., R. Vogt, and C. Körner, 2010: Tree surface temperature in an urban environment. *Agric. For. Meteor.,* **150,** 56–62.

Martin, T. A., T. M. Hinckley, F. C. Meinzer, and D. G. Sprugel, 1999: Boundary layer conductance, leaf temperature and transpiration of *Abies amabilis* branches. *Tree Physiol.,* **19,** 435–443.

Marty, C., and R. Philipona, 2000: The clear-sky index to separate clear-sky from cloudy-sky situations in climate research. *Geophys. Res. Lett.,* **27,** 2649–2652.

Müller, M. D., and D. Scherer, 2005: A grid- and subgrid-scale radiation parameterization of topographic effects for mesoscale weather forecast models. *Mon. Wea. Rev.,* **133,** 1431–1442.

Nunez, M., and T. R. Oke, 1976: Long-wave radiative flux divergence and nocturnal cooling of the urban atmosphere. *Bound.-Layer Meteor.,* **10,** 121–135.

——, and ——, 1977: The energy balance of an urban canyon. *J. Appl. Meteor.,* **16,** 11–19.

Perrier, A., 1971: Leaf temperature measurement. *Plant Photosynthetic Production: Manual of Methods,* Z. Sesták, J. Catsky, and P. G. Jarvis, Eds., Junk, 632–671.

Petty, G. W., 2006: *A First Course in Atmospheric Radiation*. 2nd ed. Sundog Publishing, 459 pp.

Plüss, C., and A. Ohmura, 1997: Longwave radiation on snow-covered mountainous surfaces. *J. Appl. Meteor.,* **36,** 818–824.

Pomeroy, J. W., D. Marks, T. Link, C. Ellis, J. Hardy, A. Rowlands, and R. Granger, 2009: The impact of coniferous forest temperature on incoming longwave radiation to melting snow. *Hydrol. Processes,* **23,** 2513–2525.

Potter, B. E., and J. A. Andresen, 2002: A finite-difference model of temperatures and heat flow within a tree stem. *Can. J. For. Res.,* **32,** 548–555.

Price, A. G., and D. E. Petzold, 1984: Surface emissivities in a boreal forest during snowmelt. *Arct. Alp. Res.,* **16,** 45–51.

Rutter, A. J., 1967: An analysis of evaporation from a stand of Scots pine. *International Symposium on Forest Hydrology,* W. E. Sopper and H. W. Lull, Eds., Pergamon Press, 403–417.

——, 1968: Water consumption by forests. *Water Deficits and Plant Growth,* T. T. Kozlowski, Ed., Vol. 2, Academic Press, 23–84.

Sedlar, J., and R. Hock, 2009: Testing longwave radiation parameterizations under clear and overcast skies at Storglaciären, Sweden. *Cryosphere,* **3,** 75–84.

Sicart, J. E., R. L. H. Essery, J. W. Pomeroy, J. Hardy, T. Link, and D. Marks, 2004: A sensitivity study of daytime net radiation during snowmelt to forest canopy and atmospheric conditions. *J. Hydrometeor.,* **5,** 774–784.

——, J. W. Pomeroy, R. L. H. Essery, and D. Bewley, 2006: Incoming longwave radiation to melting snow: Observations, sensitivity and estimation in northern environments. *Hydrol. Processes,* **20,** 3697–3708.

Spittlehouse, D. L., R. S. Adams, and R. D. Winkler, 2004: Forest, edge and opening microclimate at Sicamous Creek. British Columbia Ministry of Forests Research Program Res. Rep. 24, 55 pp. [Available online at http://www.for.gov.bc.ca/hfd/pubs/Docs/Rr/Rr24.pdf.]

Spronken-Smith, R., and T. R. Oke, 1998: The thermal regime of urban parks in two cities with different summer climates. *Int. J. Remote Sens.,* **19,** 2085–2104.

Staley, D. O., and G. M. Jurica, 1970: Flux emissivity tables for water vapour, carbon dioxide and ozone. *J. Appl. Meteor.,* **9,** 365–372.

Tan, C. S., T. A. Black, and J. U. Nnyamah, 1978: A simple diffusion model of transpiration applied to a thinned Douglas-fir stand. *Ecology,* **59,** 1221–1229.

Vanderwaal, J. A., and H. R. Holbo, 1984: Needle-air temperature differences of Douglas-fir seedlings and relation to microclimate. *For. Sci.,* **30,** 635–644.

Yamaoka, Y., 1958: The total transpiration from a forest. *Trans. Amer. Geophys. Union,* **39,** 266–272.